2019 International Conference on Industrial Engineering, Applications and Manufacturing (ICIEAM)

Thermal Analysis of an Induction Motor Subjected to Inter-Turn Short-Circuit Failures in the Stator Windings

Ananias C. P. Muxiri, Fernando Bento, D. S. B. Fonseca, Antonio J. Marques Cardoso
CISE - Electromechatronic Systems Research Centre, Universidade da Beira Interior
Calçada Fonte do Lameiro, P – 6201-001 Covilhã, Portugal
pinheiro.muxiri@ubi.pt, fjfbento@ieee.org, davide.fonseca@ieee.org, ajmcardoso@ieee.org

***Abstract*—As the main workforce of the global industry, it is fundamental to clearly understand all failures modes that may potentially deteriorate induction motors. Condition monitoring methodologies based on the thermal analysis of induction motors have tremendous potential as a health monitoring tool of any electric motor technology. In addition to the intrinsic benefits related to a non-invasive diagnostic technique, thermal analysis provides suitable information for the early detection of a plethora of fault scenarios. One of the fault modes which remains fairly unexploited in the literature is the short-circuit fault between turns of the stator windings. To assess the effects of such faults in the temperature of the stator windings of an induction motor, this paper develops a thermal model of the induction motor under study, resorting to the Finite Elements Method (FEM). To develop the FEM model, the simulation tool Flux2D (Cedrat) is employed. Distinctive fault severity levels are considered through the variation of the short-circuit resistance.**

Keywords— Condition monitoring, induction motor, thermal analysis, inter-turn short-circuit.

I. Introduction

Electric motors develop an important role in an endless number of industry applications. It is estimated that 44 % to 46 % of the electric energy consumed worldwide is used by electric motor drives [1]. Within the aforementioned group, industry is the most representative activity sector. Nearly 64 % of the electricity consumption in industry is related to electric motor drives [1].

Stator failures are among the most common fault phenomena occurring in induction machines. For low voltage machines, stator faults account for about 9 % of the total number of failures; in medium voltage machines this value rises to 35/40 %, while in high voltage machines this value reaches up to 65 % [2].

Of particular interest is the analysis of the temperature distribution inside the motor. High operating temperatures and abnormally hot spots strongly affect the machine performance and its reliability. In general, the windings' insulation is the element of the induction motor showing the lowest capability to withstand extremely high temperatures. Indeed, the rate of degradation of the windings' insulation depends on the temperature: the highest the windings temperature, the higher the rate of degradation of the insulation [3]. The materials employed in the windings' insulation are ranked based on the thermal capability. Classes are used to define the thermal capability of the insulation materials. Class F insulation materials, for instance, can withstand temperatures of up to 155 ºC [4].

The relation between the temperature and the potentially harmful effects on the machine lifetime have been studied in the past. According to the Montsinger rule, a 10 °C increment of the temperature of the winding insulation material above its rated value leads to a decrease of about 50 % in the insulation lifetime [4]–[6].

One of the most noticeable and critical effects of the degradation of the windings' insulation is the occurrence of inter-turn short-circuit faults. These faults commonly begin limited in space and severity, but quickly spread to neighboring elements. Most common effects of such faults include overheating, unbalance of the magnetic circuit, vibration and, ultimately, bearing faults [7].

The inter-turn short-circuit fault commonly arises as a consequence of the aging process of the machine windings' insulation. Thermal overload is often the cause of the windings' insulation aging process [8]. Thermal overload phenomenon may arise as a consequence of multiple operating conditions [3]:

1) Deposition of damaging agents in the motor, such as dust, humidity, oil or rust;

2) Abnormal increment of the voltage amplitude, which lead to additional losses in the machine iron core;

3) Unbalance of the motor power supply, responsible for the increment of the stator currents and, consequently, of the Joule losses on the stator windings;

4) Regular start-ups and shut-downs of the motor, over short periods of time;

5) Mechanical overload.

As one of the most severe fault modes prone to occur in induction motors, particularly the motors operating under heavy duty and harsh environmental conditions, the inter-turn short-circuit fault is also one of the fault modes of induction motors which lacks proper diagnostic tools for the correct early identification of the fault. Since local overheating is one

This work was supported by the European Regional Development Fund (ERDF) through the Operational Programme for Competitiveness and Internationalization (COMPETE 2020), under Project POCI-01-0145-FEDER-029494; and by National Funds through the FCT - Portuguese Foundation for Science and Technology, under Projects PTDC/EEI-EEE/29494/2017, UID/EEA/004131/2013, and SFRH/BD/131002/2017.

978-1-5386-8119-0/19/$31.00 ©2019 IEEE

of the most notorious symptoms of inter-turn short-circuit faults, the thermal analysis of induction motors may provide an alternative and effective tool to properly identify such faults. It is relevant to fully understand how inter-turn short-circuit faults of different severity levels affect the temperature of induction machines. Accordingly, next sections provide a detailed explanation on the development and implementation the finite elements method (FEM) to the modeling of an induction motor while subjected to inter-turn short-circuit faults.

II. Finite Elements Model

The FEM model of the induction motor under study was developed resorting to the software tool Flux2D (Cedrat).

Fig. 1 depicts the 2D geometry of the motor, used in Flux2D software. Each motor element is properly labelled in the figure.

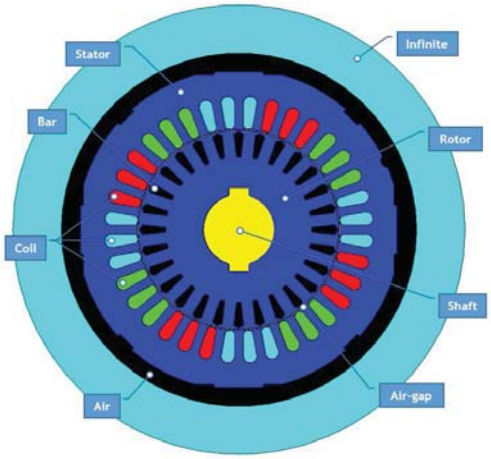

Fig. 1. 2D motor geometry.

TABLE I provides the most relevant technical parameters of the motor considered for this study.

TABLE I. Technical Parameters of the Induction Motor

General	Power [kW]	2.2
	Speed [rpm]	1435
	Frequency [Hz]	50
	Torque [Nm]	14.6
	Voltage [V]	400, star connection
	Current [A]	4.56, star connection
	Number of poles	4
	Cooling	Closed motor with external ventilation – IC 411
Stator	Turns per phase	216
	Inner diammeter [mm]	100
	Outer diammeter [mm]	160
	Number of slots	36
Rotor	Inner diammeter [mm]	35
	Outer diammeter [mm]	99.4
	Number of bars	28
	Conductor gauge [mm]	0.8 / 0.7
Winding	Pitch	1:8:10/1:8
	Layer	Single
	Per phase resistance [Ω]	2.1 (at 20 ºC)
	Insulation class	F

To obtain the map of the temperature distribution inside the motor, a two-stage procedure is adopted. The electromagnetic behaviour is initially simulated to acquire data of the losses occurring in each element of the motor. Iron losses, Joule losses and additional losses are computed through the electromagnetic simulation. To obtain the iron losses, the software Flux2D employs the Bertotti method. Then, the losses are introduced as inputs of the thermal simulation, thus allowing to simulate the evolution in time of the temperature in a cross-sectional 2D plane of the motor.

Note that both simulations are developed considering a transient state analysis, where a time domain evolution is considered.

A. Electromagnetic Simulation

Fig. 2 depicts the electric circuit used for the electromagnetic simulation. Instead of representing the windings of each phase resorting to a single circuit element, the windings of each phase are split into multiple identical coils. The windings of phase W, for instance, are represented by coils *B1*, *B2*, …, *B9* (refer to Fig. 2). Excluding coils *B1*, *B2*, and *B3*, each coil depicted in the circuit embraces 36 turns. Meanwhile, coil *B1* includes 6 turns, coil *B2* includes 9 turns, and coil *B3* includes 21 turns.

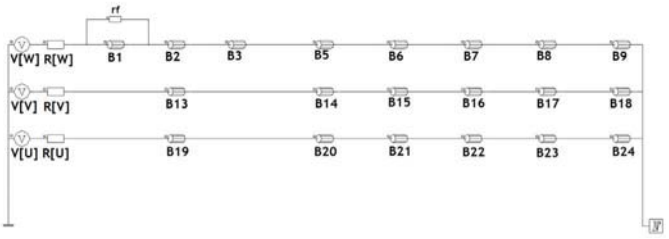

Fig. 2. Scheme of the motor electric circuit implemented at Flux2D, including the short-circuited turns at phase W.

The short-circuit condition is imposed at phase W, in coil *B1*. To obtain a controlled short-circuit condition, resistor *rf* (refer to Fig. 2) is connected in parallel with the short-circuited turns.

All simulated scenarios concern the motor operation at half load condition. The motor rated speed (1435 rpm) is considered. The load torque is set at 7 Nm, corresponding to 50 % of the rated load torque. For the electromagnetic transient analysis, the amplitude of the motor supply voltage is set as the variable in the time domain. TABLE II summarizes the parameters introduced as inputs of the electromagnetic simulation.

TABLE II. Parameters of the Electromagnetic Simulation

Load torque	7 [Nm]
Speed	1435 [rpm]
Phase U Voltage	$\frac{400}{\sqrt{3}}\times\sqrt{2}\times\sin(\omega t)$ [V]
Phase V Voltage	$\frac{400}{\sqrt{3}}\times\sqrt{2}\times\sin\left(\omega t+\frac{2\pi}{3}\right)$ [V]
Phase W Voltage	$\frac{400}{\sqrt{3}}\times\sqrt{2}\times\sin\left(\omega t-\frac{2\pi}{3}\right)$ [V]

B. Thermal Simulation

To carry out the thermal simulation, the geometry employed in the electromagnetic simulation is reused. The values of the losses computed in the electromagnetic simulation environment are used as inputs of the thermal simulation. At the initial instant of the simulation, the motor temperature is homogeneous and equal to the room temperature (25 ºC).

TABLE III provides the thermal properties of each one of the motor materials.

TABLE III. THERMAL PROPERTIES OF THE MOTOR MATERIALS

Face	Material	Thermal conductivity	Thermal inertia
Stator windings	Cooper	388 $W.m^{-1}.ºC^{-1}$	3441900 $J.m^{-3}.ºC^{-1}$
Rotor bars	Aluminum	210 $W.m^{-1}.ºC^{-1}$	2429010 $J.m^{-3}.ºC^{-1}$
Stator	Silicon steel	39 $W.m^{-1}.ºC^{-1}$	3800000 $J.m^{-3}.ºC^{-1}$
Airgap	Air	0.03 $W.m^{-1}.ºC^{-1}$	1214.4 $J.m^{-3}.ºC^{-1}$
Copper insulation	Insulation	0.083 $W.m^{-1}.ºC^{-1}$	1456000 $J.m^{-3}.ºC^{-1}$

Along with the thermal properties of the motor materials, it is critical to properly tune the coefficients that define the rate of heat transfer in boundary regions, either through convection and radiation mechanisms. The major share of heat produced inside the motor is transferred to the surrounding environment through forced convection. The selected convection coefficient should take into consideration the motor ventilation system specifications, such as speed and direction of the air flow, and the environment temperature [9]. To express forced convection conditions, the convection coefficient of the air is typically selected between 20 and 300 $W.m^{-2}.ºC^{-1}$ [10]. In this study, the convection coefficient is selected at 80 $W.m^{-2}.ºC^{-1}$. This convection coefficient is selected based on experimental tests that resort to the induction motor modelled via FEM.

Furthermore, the absorption and emissivity coefficient of the silicon steel of the stator is set at 0.95.

III. SIMULATION RESULTS

A. Electromagnetic Simulation

To determine how the severity of the short-circuit condition impacts the electromagnetic behaviour of the induction motor, four distinctive operation scenarios are considered:

- Healthy condition;
- Short-circuit of 6 turns, $rf = 1.35\ \Omega$;
- Short-circuit of 6 turns, $rf = 0.1\ \Omega$;
- Short-circuit of 6 turns, $rf = 0.001\ \Omega$.

The operation under healthy condition is considered as the reference scenario. Three other scenarios provide results for the motor operation under short-circuit fault conditions. The fault severity is controlled through the variation of the short-circuit resistance *rf* (refer to Fig. 2). In all three scenarios, the short-circuit embraces 6 turns of phase W.

TABLE IV shows the simulation results for the phase currents and short-circuit branch currents.

TABLE IV. SIMULATION RESULTS FOR THE PHASE AND SHORT-CIRCUIT CURRENTS, AS A FUNCTION OF THE SHORT-CIRCUIT RESISTANCE

	rf			
	inf. (healthy motor)	1.35 Ω	0.1 Ω	0.001 Ω
I_U	3.1 A	3.11 A	3.5 A	4.13 A
I_V	3.07 A	3.07 A	3 A	2.96 A
I_W	3.1 A	3.16 A	3.45 A	3.84 A
I_{rf}	-	4.68 A	32.1 A	63.1 A
$I_W - I_{rf}$	-	3.41 A	30.2 A	59.4 A

As a consequence of the short-circuit condition, there is a slight unbalance between the three phase currents – I_U, I_V, and I_W – as shown in TABLE IV. Such unbalance is not particularly affected by the severity of the short-circuit, since the unbalance between phases remains quite similar for all simulated scenarios. On the other hand, the current on the short-circuit resistor rises exponentially as the short-circuit resistance drops.

TABLE V presents the results of the computation of the Joule losses and iron losses, obtained through the electromagnetic simulation. Please note that TABLE V provides information on the Joule losses occurring on the short-circuited turns and on the healthy turns, separately. For the short-circuited turns, information on the Joule losses is provided in column 'Phase W (B1)'; while for the healthy turns, information is provided in column 'Phase W (B2 to B9)'.

TABLE V. MOTOR LOSSES UNDER HEALTHY AND FAULTY CONDITION

	Joule Losses [W]					Iron Losses [W]	
	Phase U	Phase V	Phase W (B1)	Phase W (B2 to B9)	Rotor bars	Stator	Rotor
rf=inf.	19.83	18.60	19.88		12.87	16.95	1.76
rf=1.35 Ω	37.80	36.72	1.14	39.96	13.52	17.58	2.72
rf=0.1 Ω	48.30	36.00	89.90	47.76	15.93	17.67	2.96
rf=0.001 Ω	66.76	35.09	348.04	59.22	19.17	17.87	3.62

As confirmed in TABLE V, the increment of the Joule losses in the stator windings, as well as in the short-circuit branch, is the most noticeable effect of the short-circuit condition. As a consequence of the short-circuit condition, there is an exponential increment of the Joule losses. Such increment is particularly sharp in the branch responsible for the short-circuit, denoted as *rf*. Still, the increment of the Joule losses in the stator windings is also noteworthy. For the scenario of a short-circuit with a resistance of 1.35 Ω, the Joule losses in the stator windings are about twice as high when compared to the healthy scenario. Moreover, the short-circuit condition promotes a non-uniform distribution of the Joule losses between the motor phases.

B. Thermal Simulation

Due to the large data sets produced while running the thermal simulations, the analysis of the simulation results will solely focus on the analysis of the temperature distribution inside the motor at the instants in which the thermal steady state is reached. According to IEEE and IEC standards, the thermal steady state of electrical machines is reached when the temperature increment along one hour is less than 2 °C [11], [12]. In this context, an analysis based on the observation and relative comparison of scenarios will be employed.

Fig. 3 to Fig. 6 depict the temperature distribution inside the motor, in °C, considering the motor operation under healthy and faulty conditions. Note that the temperature distributions presented in Fig. 3 to Fig. 6 refer to the instant of time at which

the thermal steady state condition was already met. In the conditions of load torque and initial room temperature defined for the simulations, the thermal steady state conditions are observed before the instant t = 8000 seconds.

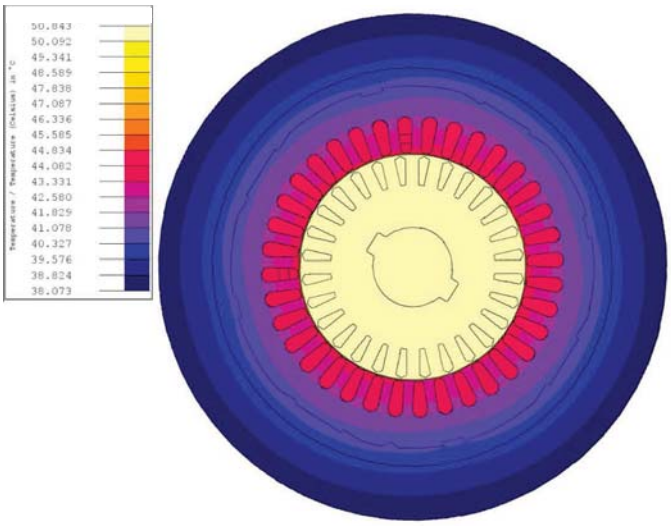

Fig. 3. Temperature distribution inside the induction motor, at t = 8000 s, considering a healthy motor condition.

As depicted in Fig. 3, there is a consistent and uniform distribution of temperatures inside the motor, typical of a healthy operation scenario. As expected, the rotor is the warmer part of the motor, followed by the stator. The rotor temperature is indeed quite uniform. Inside the stator, the windings are slightly warmer than the rest of the stator elements. Meanwhile, it is also observed that the temperature of the stator iron smoothly decreases in the direction of the stator outer boundaries.

Fig. 4 depicts the temperature distribution map inside the motor for the scenario in which a short-circuit fault between 6 turns of phase W is imposed. The short-circuit resistance (1.35 Ω) is adjusted so that the short-circuit current flowing through the short-circuit branch equals the motor rated current.

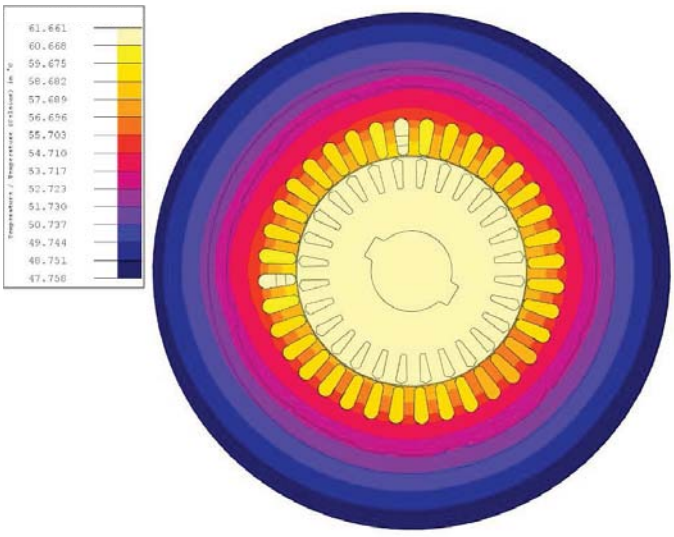

Fig. 4. Temperature distribution inside the induction motor, at t = 8000 s, considering a faulty motor condition. The short-circuit resistance is set at 1.35 Ω.

When comparing the results of Fig. 4 with the healthy condition (Fig. 3), it is observed that there is a general increment of the motor temperature. All motor components experience an increment of temperature of up to 10 °C. The rotor remains as the warmer component of the motor. As a consequence of the short-circuit fault, the temperature distribution along the stator is not uniform any longer. The slots that host the faulty turns are 2 - 4 °C warmer than all the other stator slots. The neighboring slots also suffer a minor temperature increment. The progressive decrement of temperature in the direction of the stator outer boundary is maintained in this fault condition. If a thermal analysis to the external boundary of the motor stator was carried out, the effects of the fault would remain undetected from outsider

Fig. 5 depicts the temperature distribution map inside the motor for the scenario in which a short-circuit fault between 6 turns of phase W is imposed, with a short-circuit resistance of 0.1 Ω.

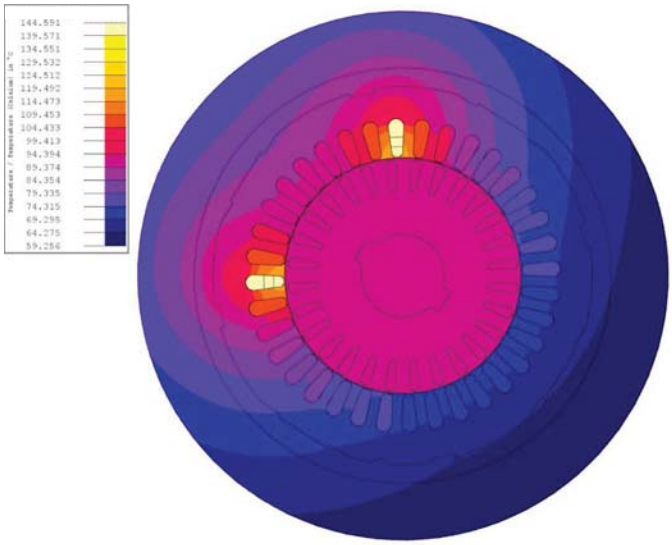

Fig. 5. Temperature distribution inside the induction motor, at t = 8000 s, considering a faulty motor condition. The short-circuit resistance is set at 0.1 Ω.

As stated in Fig. 5, the increment of the short-circuit severity promotes a sharp increment of the motor temperature, extensive to all motor components. Unlike the previous fault scenario (refer to Fig. 4), the slots that host the short-circuited turns are warmer than the rotor. Moreover, the temperature distribution along the stator is far more unbalanced than in the previous fault scenario (refer to Fig. 4). The temperature gradient between the slots that contain the faulty turns and the surrounding stator elements is greatly amplified. As a result, the progressive decrement of temperature in the direction of the stator outer boundary disappears. In this case, a simple observation of the stator surface temperature would allow to clearly notice the thermal unbalance along the stator. Despite the severe increment of temperature occurring near the short-circuited turns, the temperature of the warmest regions remains slightly below the critical temperature, at which the integrity of the windings' insulation is sustained (155 °C).

Fig. 6 depicts the temperature distribution map inside the motor for the scenario of a pure short-circuit between 6 turns of phase W.

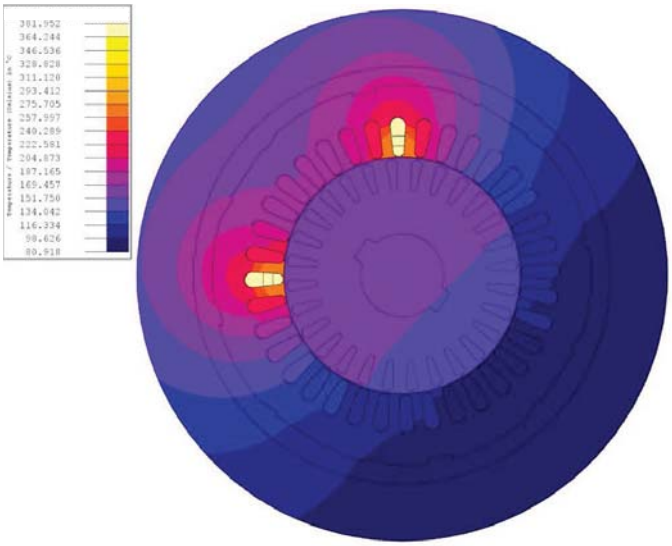

Fig. 6. Temperature distribution inside the induction motor, at t = 8000 s, considering a faulty motor condition. The short-circuit resistance is set at 0.001 Ω.

As witnessed in Fig. 6, the condition with lowest short-circuit resistance leads to a massive overheating of the windings located nearby the short-circuited turns. Even though the excessive heating is pretty much concentrated in space, such overheating also spreads to the rest of the stator and to the rotor, leading to a non-uniform heating of the motor. Since the insulation class of the motor windings is class F, the motor would fail well before verifying such a violent short-circuit condition. Just like in the previous scenario (refer to Fig. 5), the distribution of the stator surface temperature would not be uniform.

IV. Conclusions

This paper develops an analysis of the effects of inter-turn short-circuit faults in the temperature of the induction motor. Overall, a massive increment of the temperature in the motor stator windings is experienced when this type of fault occurs. The severity of the motor overheating is particularly expressive and localised in space when the short-circuit resistance is low. Furthermore, such condition also promotes an unbalanced distribution of the temperature inside the motor. According to the simulation results, such unbalance in the temperature distribution inside the motor can be either noticed from outside. Hence, a thermographic analysis, based on a thermal camera, can be employed in motors that do not have any temperature sensors inside, while enabling an online non-invasive analysis.

References

[1] P. Waide and C. U. Brunner, “Energy-Efficiency Policy Opportunities for Electric Motor-Driven Systems,” *IEA Energy Papers*, no. 2011/07, p. 39, 2011.

[2] K. N. Gyftakis, M. Sumislawska, D. F. Kavanagh, D. A. Howey, and M. D. McCulloch, “Dielectric Characteristics of Electric Vehicle Traction Motor Winding Insulation under Thermal Aging,” *IEEE Transactions on Industry Applications*, vol. 52, no. 2, pp. 1398–1404, March-April 2016.

[3] A. J. M. Cardoso, *Diagnóstico de Avarias em Motores de Indução Trifásicos*. Coimbra Editora (ISBN 972-32-0452-5), Coimbra, Portugal, 1991.

[4] A. M. S. Mendes, X. M. López-Fernández, and A. J. Marques Cardoso, “Thermal Performance of a Three-Phase Induction Motor Under Fault Tolerant Operating Strategies,” *IEEE Transactions on Power Electronics*, vol. 23, no. 3, pp. 1537–1544, May 2008.

[5] H. Oraee, “A Quantative Approach to Estimate the Life Expectancy of Motor Insulation Systems,” *IEEE Transactions on Dielectrics and Electrical Insulation*, vol. 7, no. 6, pp. 790–796, Dec. 2000.

[6] B. Baptista, A. Mendes, S. Cruz, and A. Cardoso, “Temperature Distribution Inside a Three-Phase Induction Motor Running with Eccentric Airgap,” *Electrical Review*, no. 1, pp. 96–99, Jan. 2012.

[7] G. K. Singh and S. A. S. Al Kazzaz, “Induction Machine Drive Condition Monitoring and Diagnostic Research - A Survey,” *Electric Power Systems Research*, vol. 64, no. 2, pp. 145–158, Feb. 2003.

[8] M. Sumislawska, K. N. Gyftakis, D. F. Kavanagh, M. D. McCulloch, K. J. Burnham, and D. A. Howey, “The Impact of Thermal Degradation on Properties of Electrical Machine Winding Insulation Material,” *IEEE Transactions on Industry Applications*, vol. 52, no. 4, pp. 2951–2960, July-Aug. 2016.

[9] D. Staton, A. Boglietti, and A. Cavagnino, “Solving the More Difficult Aspects of Electric Motor Thermal Analysis in Small and Medium Size Industrial Induction Motors,” *IEEE Transactions on Energy Conversion*, vol. 20, no. 3, pp. 620–628, Sept. 2005.

[10] Convection Heat Coefficient [Online]. Available: http://help.solidworks.com/2012/english/solidworks/cworks/convection_heat_coefficient.htm.

[11] IEEE Power Engineering Society, IEEE Standard Test Procedure for Polyphase Induction Motors and Generators, IEEE Std 112 - 2004, Revision of IEEE Std 112-1996.

[12] IEC 60034-1, twelfth edition, 2010, Rotating electrical machines – Part 1: Rating and performance.